Engineered Science
DOI: https://dx.doi.org/10.30919/es921

Data-driven Modeling for Stability Evaluation of Cylindrical Boreholes with Slurry in Anisotropic and Non-Homogeneous Clays

Khamnoy Kounlavong,[1] Jim Shiau,[2] Van Qui Lai,[3,4] Vinay Bhushan Chauhan,[5] Pitthaya Jamsawang[6] and Suraparb Keawsawasvong[7,*]

Abstract

Wet-bored pile construction is a commonly used technique by contractors for building bored piles. This method involves the use of a special drilling fluid, known as bentonite slurry, to support the borehole walls and prevent their collapse during the drilling process. Given the importance of such a soil stability problem, the present paper aims to study borehole stability and its associated failure mechanisms of all relevant design parameters. In particular, we focus on the investigation of the depth and diameter of the cylindrical borehole for anisotropic and non-homogeneous clays. To achieve this goal, the advanced finite element limit analysis (*FELA*) method alongside the upper and lower bounds limit analysis is used as a numerical tool to perform a series of the parametric study. The dimensionless variables utilized in this study consist of a practical range of depth ratio (H/D), dimensionless strength gradient ($\rho H/S_{uc0}$), and anisotropic strength ratio (r_e). The newly obtained numerical results are in good agreement with previous studies, and therefore several design charts are confidently produced for the design of cylindrical borehole stability using a dimensionless stability number. The study continues to explore the associated failure mechanisms using the graphical output of velocity fields. The artificial neural network (ANN), which is one of soft-computing techniques, is utilized to establish a surrogate model for predicting the borehole stability and also developing a correlation equation based on FELA results. This correlation equation is useful to practical engineers as it can be used to predict the stability number N and factor of safety (FS) in their daily design practices.

Keywords: Borehole stability; Anisotropic clay; Slurry pressure; FELA; ANN.
Received: 31 May 2023; Revised: 30 June 2023; Accepted: 30 June 2023.
Article type: Research article.

1. Introduction

Bentonite-water slurry supported borehole is commonly used during the construction process of pile or open caisson foundation. This method is preferred over pure water as it improves stability by creating lateral pressure on the borehole face. Previous studies of the problem include the limit equilibrium method (LEM) to determine the factor of safety of a borehole or planar excavation's stability in 2D plane strain trenches.[1-3] Similarly, researchers have used the LEM technique in 3D to propose the stability of 3D trenches by considering the soil arching phenomenon.[4-8] In addition, the elasto-plastic finite element method (FEM) with strength reduction has been used by Oblozinsky *et al*.[9] and Grandas-Tavera and Triantafyllid is[10] to carry out numerical solutions for slurry trench wall stability.

Han *et al*.,[11] Zhang *et al*.,[12] Qin,[13] and Wang and Huang[14] have used limit analysis procedures based on upper and lower bound theorem to determine the stability of slurry-supported trenches. Li *et al*.[15] used the finite element limit analysis (FELA)[16] numerical procedure to derive plastic solutions of 3D rectangular trenches under bentonite pressure. Additionally, several researchers have also studied unsupported cylindrical and rectangular excavations without considering slurry pressure using axisymmetric and 3D

[1] *Department of Civil Engineering, Faculty of Engineering, Thammasat School of Engineering, Thammasat University, Pathumthani 12120, Thailand.*
[2] *School of Engineering, University of Southern Queensland, Toowoomba, 4350, QLD, Australia.*
[3] *Faculty of Civil Engineering, Ho Chi Minh City University of Technology (HCMUT), 268 Ly Thuong Kiet Street, District 10, Ho Chi Minh City, Vietnam.*
[4] *Vietnam National University Ho Chi Minh City (VNU–HCM), Linh Trung Ward, Thu Duc District, Ho Chi Minh City, Vietnam.*
[5] *Civil engineering Department, Madan Mohan Malaviya University of Technology, Gorakhpur, India.*

FELA.[16-27] More recently, Keawsawasvong and Shiau[28] have presented stability solutions for boreholes with slurry in isotropic clays using axisymmetric FELA.

Ladd[29] and Ladd and Degroot[30] reported the inherent anisotropy of clayey soils, as well as stress-induced anisotropy, would cause the principal stress to rotate towards the vertical axis or the depositional direction. As a result, they defined three anisotropic undrained shear strengths using triaxial compression (S_{uc}), triaxial extension (S_{ue}), and direct simple shear (S_{us}).[31] Recently, Krabbenhoft *et al*.[32] developed a new failure criterion for anisotropic clay called the Anisotropic Undrained Shear (AUS) model by extending the generalized Tresca failure criterion.[33] Several previous studies have utilized the AUS failure criterion along with the FELA approach to solve stability problems such as bearing capacity,[34-36] pullout capacity,[37,38] and excavation and opening problems.[39]

Even though, there were few previous studies regarding the borehole stability,[40-45] most of them are case studies, where the design charts or equations were not given. To our best knowledge, there has been no prior investigation of a slurry-supported borehole in anisotropic and non-homogeneous clay. An increase in anisotropic undrained shear strength as subsurface depth increases would significantly affect cylindrical borehole stability. Therefore, this study aims to present limit analysis solutions for cylindrical borehole stability while taking into account the impacts of anisotropy and non-homogeneity of the clay. In this study, axisymmetric Finite Element Limit Analysis (FELA) with the AUS model is utilized to assess the upper bound (UB) and lower bound (LB) solutions of the aforementioned problem. The artificial neural network (ANN), as one of soft-computing techniques, is utilized to establish a surrogate model for predicting the borehole stability. In this study, ANNs are applied to generate the relationship between input data (H/D, $\rho H/S_{uc0}$, r_e) and outcome stability number. The structure of an ANN in MATLAB code refers to the input nodes, hidden layers and nodes, and the output node. R squared (R^2), Mean Absolute Error (MAE), and Root Mean Squared Error (RMSE) are extensively used as assessment metrics in Artificial Neural Networks (ANN) to analyze the performance of the trained model. Furthermore, weights and biases, the final results of ANN model adjustment and optimization, are presented, and performance and careful tuning of these parameters are crucial to attaining good results. Finally, the importance of each input variable can be estimated by examining the weights associated with each network connection. Thus, the novelty of this study is that the ANN model for predicting the cylindrical borehole stability in anisotropic and non-homogeneous clay is proposed for the first time and can be employed to assess the stability of such problem for practical engineers.

[6] *Soil Engineering Research Center, Department of Civil Engineering, King Mongkut's University of Technology North Bangkok, Bangkok 10800, Thailand.*

[7] *Department of Civil Engineering, Faculty of Engineering, Thammasat School of Engineering, Thammasat University, Pathumthani 12120, Thailand.*

Email: ksurapar@engr.tu.ac.th (S. Keawsawasvong)

2. Problem definition

Figure 1 shows a problem statement of a cylindrical borehole that has been excavated to install a pile under the influence of slurry pressure. The diagram presents a plan view of the cylindrical borehole diameter as well as a front view showing the depth of the cylindrical borehole filled with slurry, which is leveled with the depth of the cylindrical borehole. Fig. 2 depicts the geometry of a cylindrical borehole that is subjected to slurry pressure under axisymmetric conditions. The cylindrical borehole has a depth (H) and a diameter (D), and the saturated unit weight of the undrained clay is represented by γ. The slurry pressure acts on the inner surface and bottom of the cylindrical borehole and is denoted by the expression $\gamma_s H$, where γ_s is the unit weight of the slurry pressure. The undrained shear strength of non-homogeneous clays that increases linearly with depth (z) can be calculated using the equation $S_{uc}(Z) = S_{uc0} + \rho z$, where S_{uc0} is undrained shear strength at the surface and ρ is the strength gradient.

The anisotropic undrained soil (AUS) model requires three input parameters, namely, undrained shear strength in triaxial compression (S_{uc0}) and extension (S_{ue0}), as well as in direct shear (S_{us0}). These parameters can be calculated from two anisotropic strength ratios, namely $r_e = S_{ue0}/S_{uc0}$ and $r_s = S_{us0}/S_{uc0}$. To normalize the three anisotropic undrained shear strengths by combining both r_e and r_s ratios, an equation proposed by Krabbenhoft *et al*.[32] can be used, which is given as $r_s = 2r_e / (1 + r_e)$.

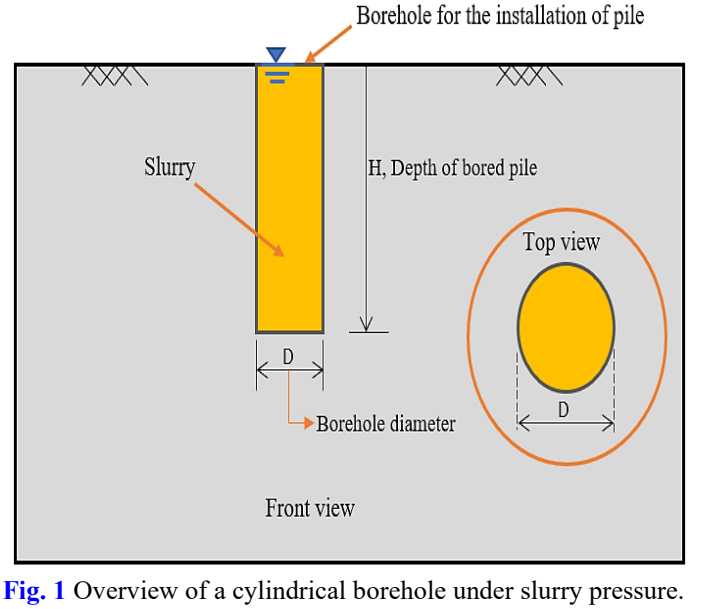

Fig. 1 Overview of a cylindrical borehole under slurry pressure.

The analysis of the upper and lower bounds solutions of cylindrical boreholes in anisotropic and non-homogeneous clays involves certain input parameters including H, D, γ, γ_s, ρ, S_{uc0}, and r_e. To obtain the stability number that can be used

to calculate the factor of safety, these input parameters are used to derive three dimensionless variables as:[46] H/D, r_e, and $\rho H/S_{uc0}$. These variables are related to the borehole stability numbers and the failure mechanisms of shear dissipations in the problem and Eq. (1) shows the relationship between these variables.

$$N = \frac{FS(\gamma - \gamma_s)H}{S_{uc0}} = f(\frac{H}{D}, r_e, \frac{\rho H}{S_{uc0}}) \quad (1)$$

where H/D is the depth ratio of the cylindrical borehole; $\rho H/S_{uc0}$ is the dimensionless strength gradient; r_e is an anisotropic strength ratio; N is the cylindrical borehole stability number. The notations of parameters used in this study are comprehensively shown in Fig. 1.

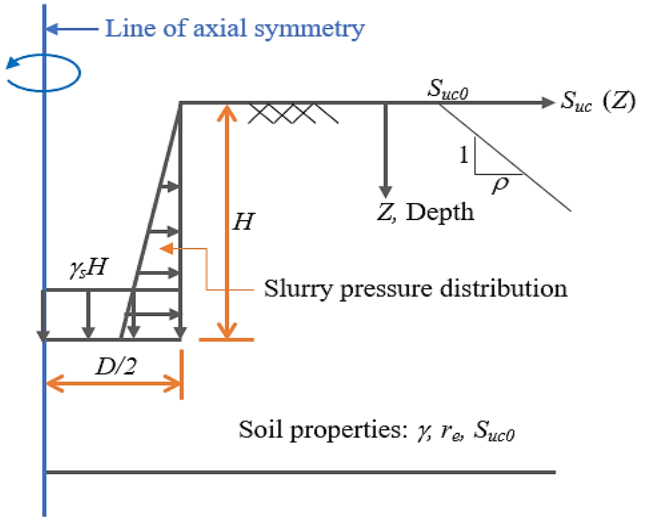

Fig. 2 Geometry problem of the cylindrical borehole under slurry pressure in axisymmetric condition.

3. Finite element limit analysis (FELA)

This study proposes to use finite element limit analysis to determine the stability number (N) as well as the associated failure mechanisms of a cylindrical borehole under axisymmetric conditions. OptumG2 software was employed to model the problem.[47] Note that the OptumG2 is based on the FELA framework providing only the limit state of geotechnical problems, which is different from the displacement-based finite element analysis that also provides the deformations.[48-52] The soil model adopted in this study is for AUS materials with considerations given to anisotropic and non-homogeneous clays. All numerical solutions used in the present study are based on the bounding theorem, which are lower and upper bounds, and they are presented throughout the paper using the average results (*i.e.*, (UB+/LB)/2). A half-cylindrical borehole model is shown in Fig. 3a, with the axial symmetry line set at the left domain, the dimensions of the domain, and the applied equivalent slurry pressure. Note that the slurry pressure is simulated as a linearly increasing pressure with depth, starting from zero at the top and reaching $\gamma_s H$ at the bottom of the cylindrical borehole.

Figure 3b shows a typical FELA mesh of the problem. To ensure that the size of the boundary domain does not affect the overall velocity field during the numerical process, the domain size in the X and Y dimensions is determined by the following expressions: $X = 1.5(H + D/2)$ and $Y = 1.5H$, respectively. If failure slip lines of problem intersect the right and bottom boundaries due to the insufficient boundary size, the accuracy of FELA solutions can be decrease. Noting that the soil movement of the bottom boundary is prevented in both vertical and horizontal directions, the left-hand side boundary is permitted to have vertical movement, simulating a line of axial symmetry. A roller type of boundary is given to the far right-handed side, and the top ground surface of the borehole is a free surface. What is interesting in the adaptive mesh given in Fig. 3b is that it can be used to improve the solution accuracy greatly. In this paper, five adaptivity steps were employed in all computations, along with the default option of using shear dissipation as the adaptive control parameter,[53] and the number of elements in the mesh increased from 5,000 in the first step to 10,000 in the final mesh. Note that the mesh is automatically expanded in sensitive zones with significant plastic shearing strain using adaptive mesh techniques. Employing more elements may indicate a more sensitive stress zone, leading to a more precise solution, but it is not necessary to use more than 10,000 elements as it may consume additional CPU time and computer memory with little effect on the solution. Note that, by using this setting of the adaptive mesh refinement, the LB and UB solutions are extremely close meaning that the true solutions can be obtained.

With the above setting for FELA, the practical range of dimensionless variables considered in the paper includes the depth ratio (H/D) at values of (0.5, 1, 2.5, 5, 10, 20, 30, and 40), the dimensionless strength gradient ($\rho H/S_{uc0}$) at values of (0, 0.5, 1, 2, and 5), and the anisotropic strength ratio (r_e) at values of (0.5, 0.6, 0.7, 0.8, 0.9, and 1). Note that the selected values of all parameters are based on the previous studies by Li *et al.*[6] and Keawsawasvong and Shiau.[28] The comprehensive numerical solutions are reported in the next section.

4. Data-driven analysis (ANN model)

Artificial Neural Network (ANN) is a computational model based on the human brain that involves creating algorithms and models that allow computers to learn from data and make predictions or judgments. McCulloch and Pitts[54] introduced the first mathematical model of an artificial neural network and provided the foundation for the development of any research on ANN. Moreover, this machine learning approach now plays an essential role in numerous areas, from the economy to engineering. The concept of the ANN model is prepared in Fig. 4 and the detail of the ANN model can be found in.[55-59]

In this study, numerical results are adopted as the feeding data for the ANN model to propose the empirical equation between investigated parameters (H/D, $\rho H/S_{uc0}$, r_e) and output stability (N). In detail, there are 270 datasets of (H/D, $\rho H/S_{uc0}$, r_e) that influence the borehole stability (N). As standard

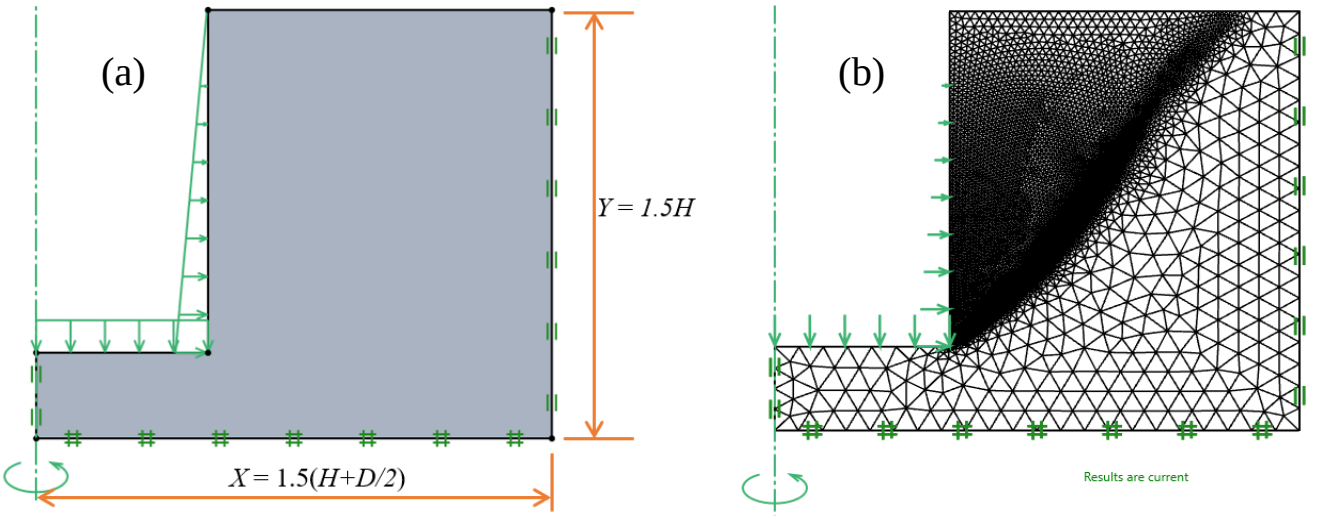

Fig. 3 (a) Numerical model of the cylindrical borehole under slurry pressure in OptumG2; (b) final adaptive mesh.

procedure, the datasets are split into three groups including training, validation, and testing with the following ratios: 70%, 15%, and 15%, respectively. Three are two important algorithms for the ANN model, *i.e.*, optimization algorithm which is used to update the weight and bias of neurons, and active function which is used to transform the weighted sum of the input and bias into the output of a node. In the present ANN model, the Levenberg-Marquardt (LM) optimization and Log-sigmoid are applied as the optimization algorithm and activation function. The detail of the LM algorithm can be referred to the works of Hagan *et al*.[60] and the Log-sigmoid activation function can see in the works of Shim *et al*..[61]

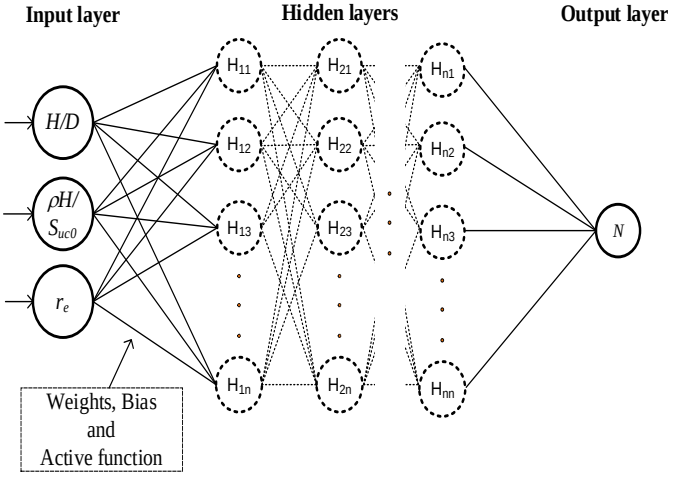

Fig. 4 Concepts of ANN model.

5. Results and discussions

5.1 Comparison

As a first step to verify the proposed model, the numerical results of this study for the case of anisotropic strength ratio, r_e = 1 are compared with published results from Keawsawasvong and Shiau.[28] Shown in Fig. 5 is the influence of *H/D* on the borehole stability number (*N*) for the various dimensionless strength gradient ($\rho H/S_{uc0}$ = 0, 0.5, 1, and 2). Numerical results have shown that the published solutions are slightly greater than our results for all the considered cases. The variation ranges are about (3-5%, 2-4%, 2-4%, and 2-4%) for corresponding values of ($\rho H/S_{uc0}$ = 0, 0.5, 1, and 2), respectively. This has greatly enhanced the confidence in producing all numerical results as follows.

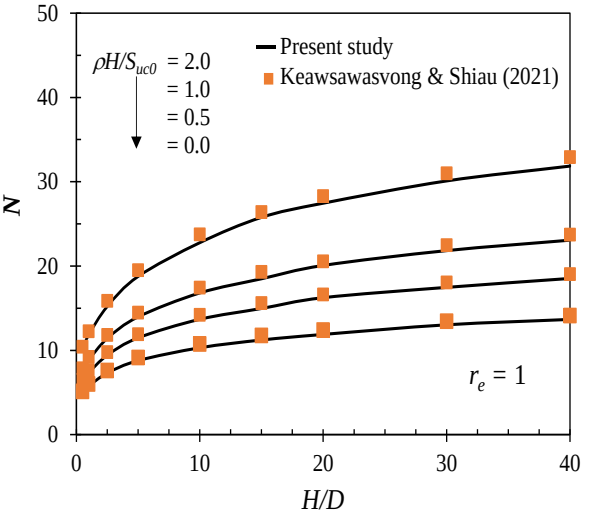

Fig. 5 Comparison between the *N* values obtained from present and past study Keawsawasvong & Shiau [28].

5.2 Parametric results

The bulk of numerical results of the dimensionless stability number (*N*) is presented in Figs. 6-8. Note that they are presented as averaging the value obtained from the lower bound (*LB*) and upper bound (*UB*) solutions. In Figs. 6a-6f, the variations of borehole stability number (*N*) with borehole depth to diameter ratio (*H/D*) are presented for the different anisotropic strength ratios (r_e) ranging from 0.5 to 1 and the dimensionless strength gradient ($\rho H/S_{uc0}$) values of (0, 0.5, 1, 2, and 5). Numerical results have shown that the borehole stability number increases nonlinearly with the increase in the *H/D* ratio. Depending on the magnitude of $\rho H/S_{uc0}$ and r_e values, the rates of increase are different. In general, the larger the ($\rho H/S_{uc0}$), the greater the gradient of the curve.

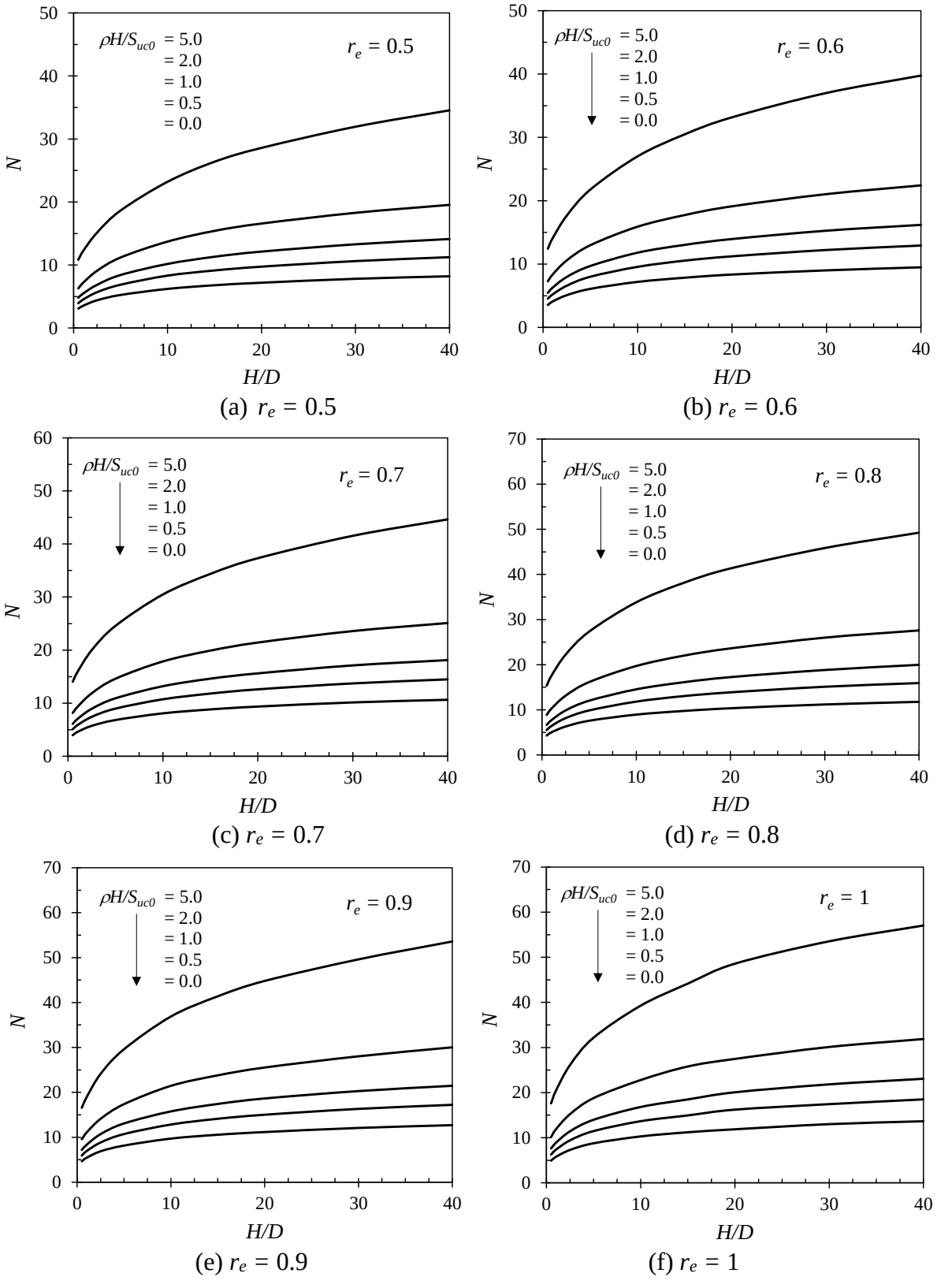

Fig. 6 Influence of *H/D* on the borehole stability number with various dimensionless strength gradients ($\rho H/s_{u0}$) and anisotropic strength ratios (r_e).

The influence of $\rho H/S_{uc0}$ on the borehole stability number (N) is shown in Figs. 7a-7f for the various depth-to-diameter ratio (H/D) and anisotropic strength ratio (r_e). The figure has shown that $\rho H/S_{uc0}$ has a significant impact on the value of N. An increase in $\rho H/S_{uc0}$ leads to a linear increase in N for all values of H/D and r_e. This behavior can be attributed to the fact that an increase in $\rho H/s_{uc0}$ results in a greater undrained shear strength of the clay surrounding the borehole, making it

more resistant to the forces acting around the borehole than in the case of homogeneous clay (*i.e.*, $\rho H/S_{uc0}$ =0). Therefore, both the value of N and the factor of safety (FS) increase with an increase in the $\rho H/S_{uc0}$ ratio. The larger the value of H/D (*i.e.*, the smaller the borehole diameter), the greater the stability number. Indeed, a smaller diameter of borehole would yield more stable results when compared to a larger diameter borehole. It is expected that a greater arching effect occurs as the value of H/D increases.

The study on the effect of anisotropic strength ratios r_e is presented in Figs. 8a-8e, where the relationship between the borehole stability number N and r_e is shown for the various values of H/D and $\rho H/S_{uc0}$. *Noting the linear* relationship between N and r_e over the entire range of H/D and $\rho H/S_{uc0}$ considered, this trend can be understood by knowing the fact that when the value of r_e is less than one ($r_e < 1$) the soil properties do not exhibit uniform strength in all directions. In the contrast, when r_e equals one ($r_e = 1$), the soil properties are such that the undrained shear strength of the clay is consistent in all directions ($S_{uc} = S_{ue} = S_{us}$). This is the reason why the borehole stability number increases with an increase in the value of r_e.

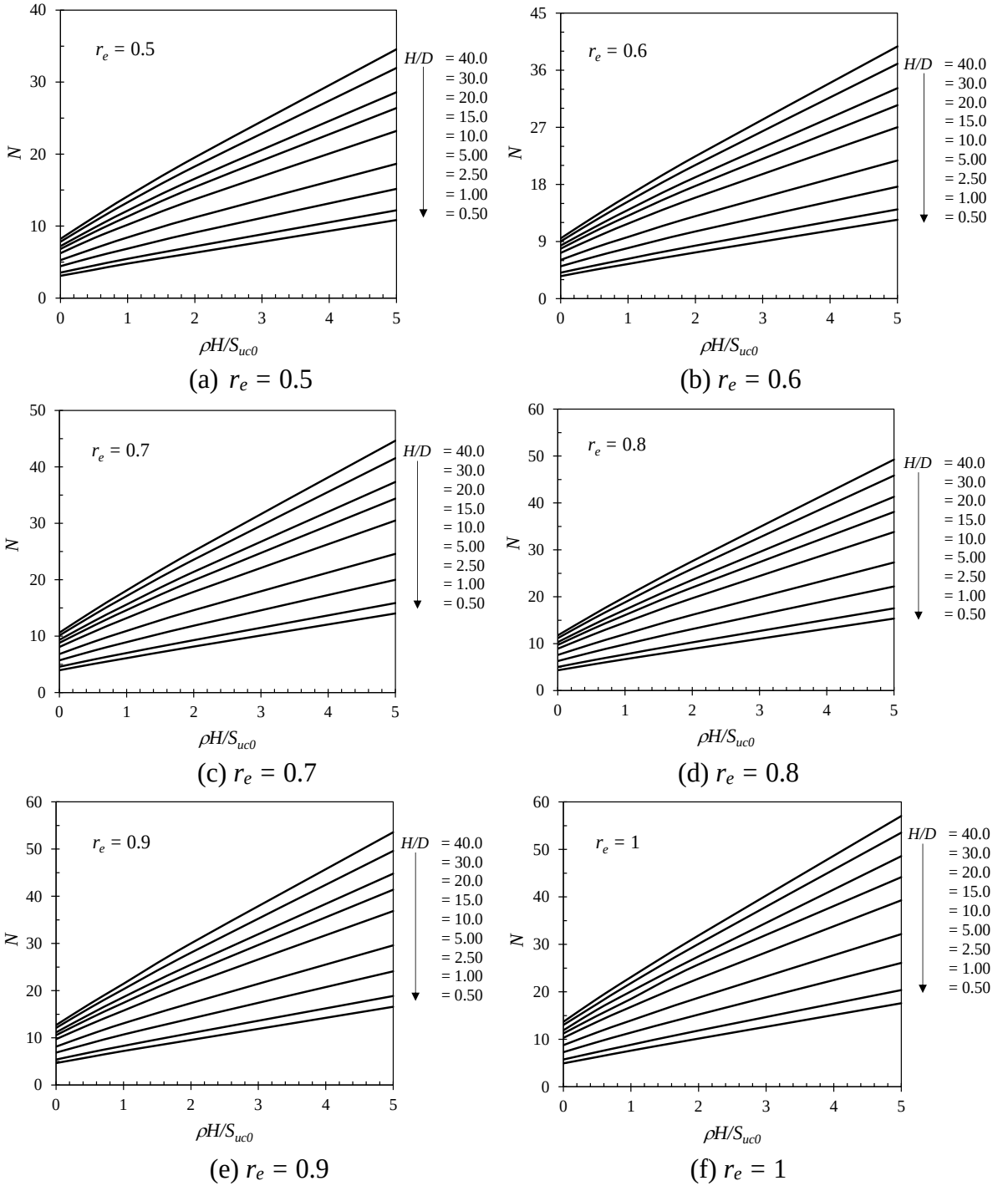

Fig. 7 Influence of $\rho H/s_{u0}$ on the borehole stability number with various depth ratios (H/D) and anisotropic strength ratios (r_e).

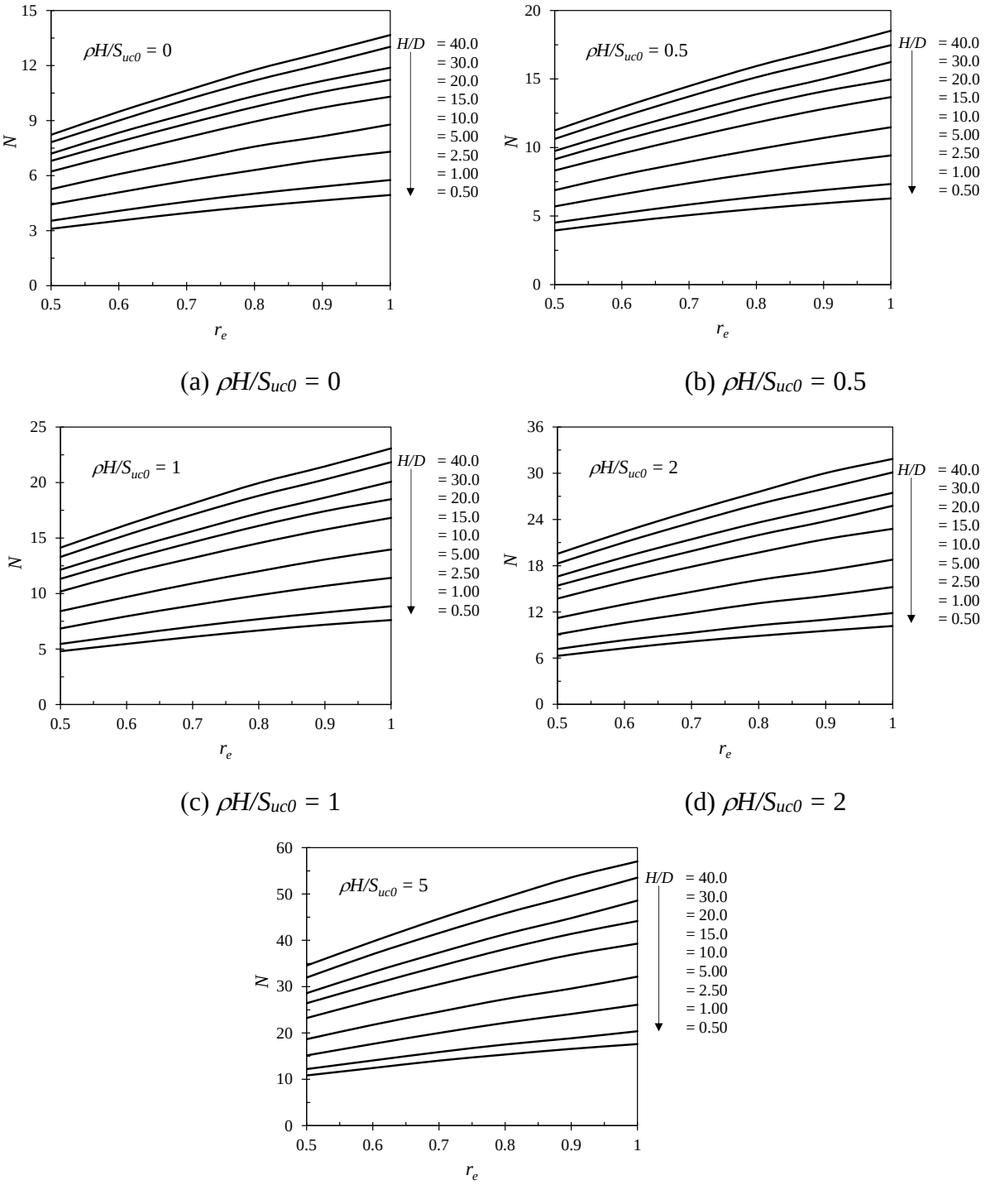

(a) $\rho H/S_{uc0}$ = 0

(b) $\rho H/S_{uc0}$ = 0.5

(c) $\rho H/S_{uc0}$ = 1

(d) $\rho H/S_{uc0}$ = 2

(e) $\rho H/S_{uc0}$ = 5

Fig. 8 Influence of r_e on the borehole stability number with various depth ratios (H/D) and dimensionless strength gradients ($\rho H/s_{u0}$).

5.3 Failure mechanisms – contour of velocity field

This section investigates potential failure mechanisms of boreholes under slurry pressure by examining the effects of (H/D, $\rho H/S_{uc0}$, and r_e). The potential failure mechanisms are expressed by using the contours of velocity fields, and the variables considered are H/D, $\rho H/S_{uc0}$, and r_e, as shown in Figs. 9-11. Note that the actual values of the color contours are not important for such a perfectly plastic material model, therefore they are not normally shown in a professional report. Yet, the most important element in presenting these color plots is simply to show the slip surfaces or the so called failure mechanism.

For the case of r_e = 0.7 and $\rho H/S_{uc0}$=1 (see Fig. 9), velocity contour plots are presented for H/D = (0.5, 1, 5, and 10) respectively. For a larger diameter, *i.e.*, a small H/D ratio as seen in the case of H/D = 0.5 and 1, failure occurs from the

borehole bottom corner and extends toward the ground surface. As H/D increases, the failure tends to confine in the local area, as seen in the case of H/D = 5 and 10, much larger velocity values occur at the borehole's bottom corner and extend forward one-third of the borehole height, resulting in a type of possible local failure.

The effect of $\rho H/S_{uc0}$ on the associated failure mechanism is shown in Figs. 10a-10d. The case considered here is for (r_e = 0.7 and H/D =1). The figures have shown that, by increasing the value of $\rho H/S_{uc0}$, it would cause the shape of the slip surface to shift from curvilinear to linear. Consequently, this results in a narrower failure zone being observed when the ratio of $\rho H/S_{uc0}$ becomes greater (*i.e.*, an increase of the gradient of the linear increase).

Finally, Figs. 11a-11d shows the influence of r_e on the potential failure slip surface of the borehole. The presented case is for (H/D = 1 and $\rho H/S_{uc0}$ = 1). It is interesting to note the two slip surfaces (see the red color) in the cases of smaller r_e values (*i.e.*, r_e = 0.5 and 0.7). This observation can be attributed to the fact that, in the case of an isotropic condition (r_e = 1, see Fig. 10d), clay properties have equal strength in all directions (S_{uc} = S_{ue} = S_{us}), resulting in only one distinct potential failure plane around the borehole, whereas, with smaller r_e values, multiple potential failure envelopes can occur.

5.4 ANN results

For analysis purposes, the optimal ANN model in other words the optimal architecture ANN model is selected. It is recognized that the simplest ANN model with one hidden layer, which was adopted in previous research, is suitably used in this study. Accordingly, the performance of investigated ANN model is exanimated through the three regression parameters *i.e.*, the coefficient of determination (R^2), the Root Mean Square Error (RMSE), and the Mean Absolute Error (MAE).

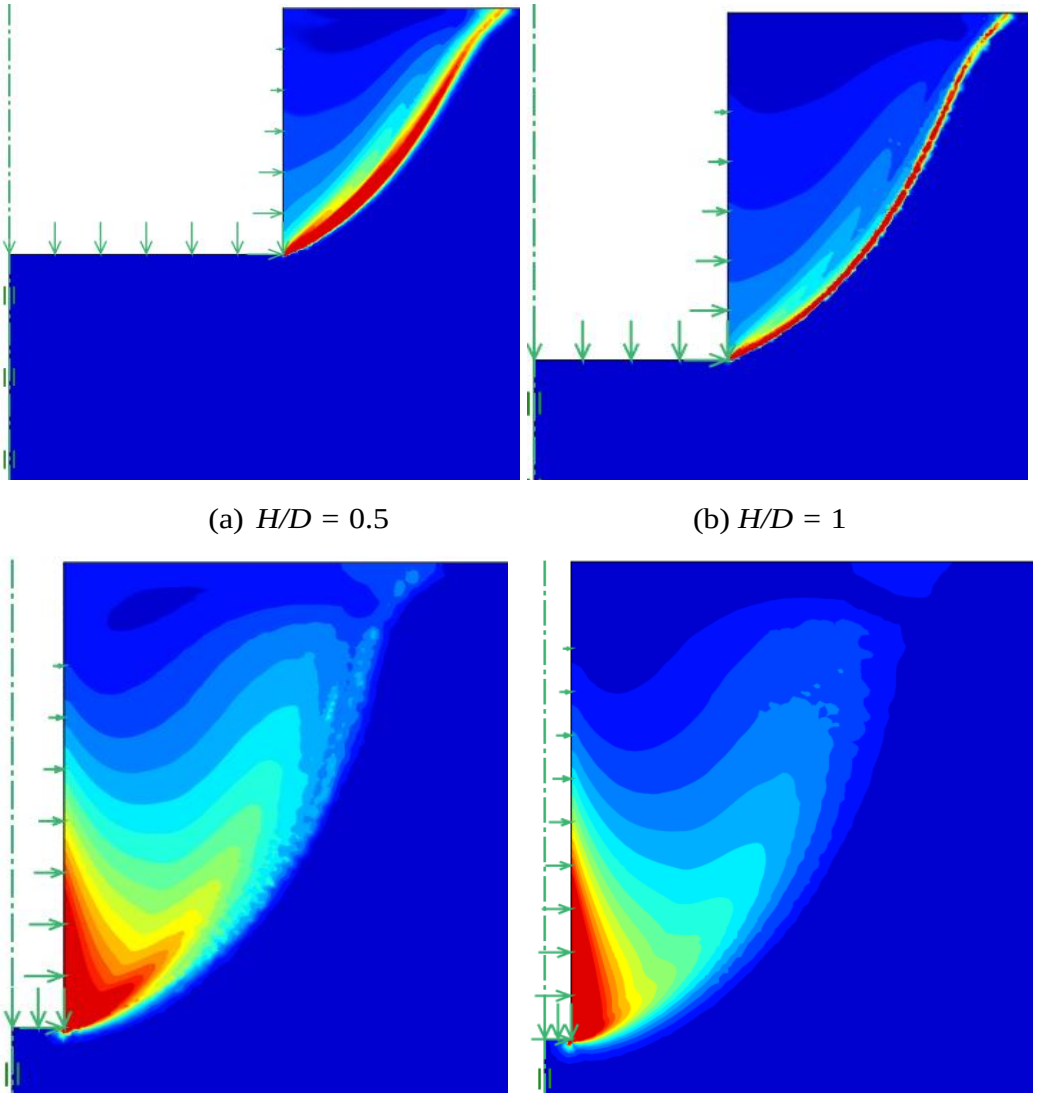

(a) H/D = 0.5 (b) H/D = 1

(c) H/D = 5 (d) H/D = 10

Fig. 9 Effect of H/D on the shear dissipations of soil, having r_e = 0.7 and $\rho H/s_{u0}$ = 1.

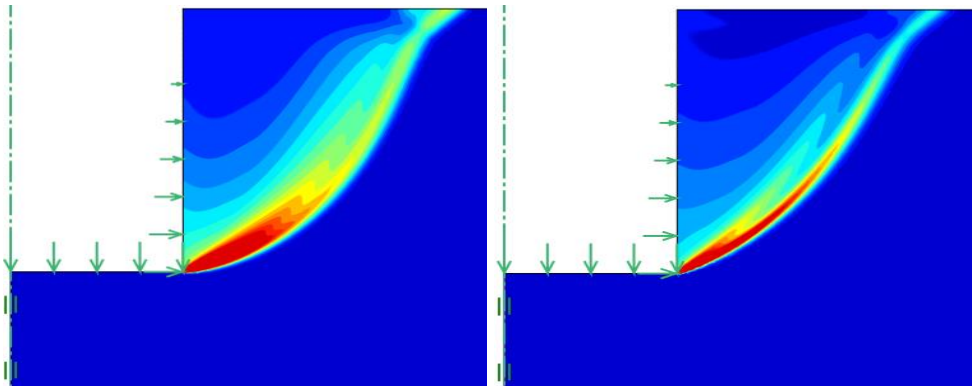

(a) $\rho H/S_{uc0} = 0$ (b) $\rho H/S_{uc0} = 1$

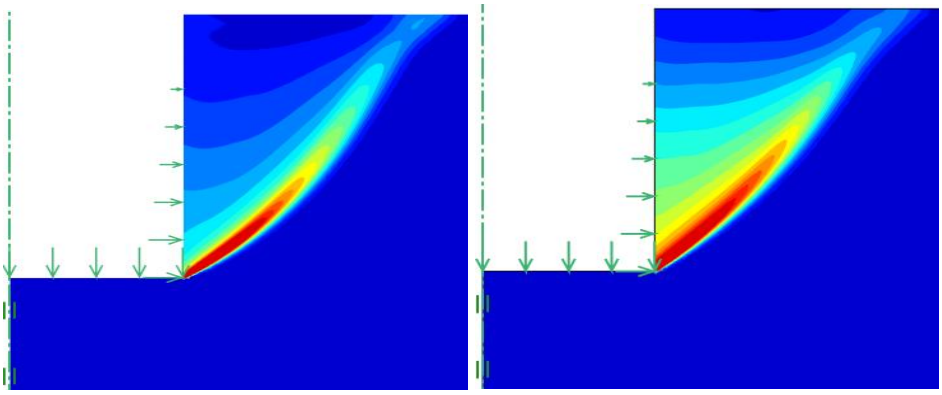

(c) $\rho H/S_{uc0} = 2$ (d) $\rho H/S_{uc0} = 5$

Fig. 10 Effect of $\rho H/s_{u0}$ on the shear dissipations of soil, having $r_e = 0.7$ and $H/D = 1$.

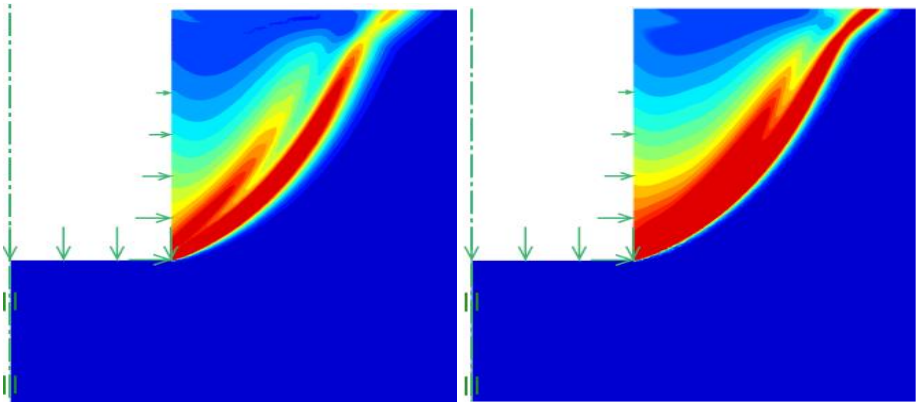

(a) $r_e = 0.5$ (b) $r_e = 0.7$

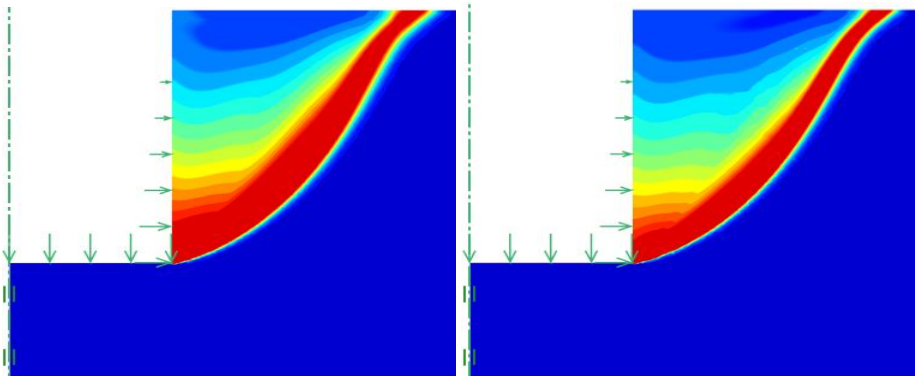

(c) $r_e = 0.9$ (d) $r_e = 1$

Fig. 11 Effect of r_e on the shear dissipations of soil, having $\rho H/s_{u0} = 1$ and $H/D = 1$.

The relationship between the number of neurons (NNs) in the hidden layer and R^2, RMSE, and (MAE) is presented in Fig. 12. The graph shows that when the number of neurons is less than 6, the coefficient R^2 does not approach approximately the optimal value of 1. Meanwhile, the value of RMSE and MAE tend to decrease to 0, but both errors are still quite large and show no sign of stabilization. This error can lead to the wrong prediction for borehole stability number results (N) in the ANN model. Hence, when the number of neurons 6 is used to train the ANN model in an optimal and stable drawing, R^2 is nearly equal to one, and RMSE and MAE are close to 0. It is essential to explain why the number of neurons was not chosen as 8 because the outcome is not significantly better than 6, but given the number of neurons running more than 2 neurons, this is not optimal and necessary.

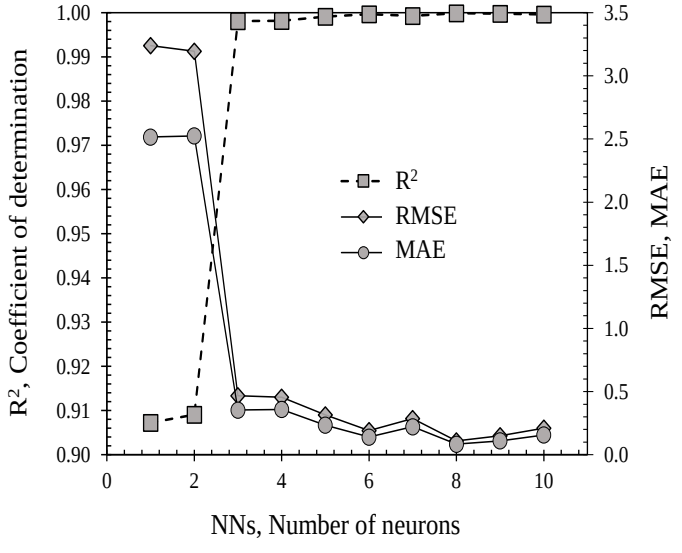

Fig. 12 The relationship between R^2, RMSE, MAE and the number of neurons.

By using the constant value of the ANN model such as weight and bias, it can build an empirical equation based on active function, as shown in Eq. (2).

$$N_n = \sum_{h=1}^{Nh} W^{23}\,\text{tansig}\left(\sum_{i=1}^{Ni} W^{12} x_{Ni} + b^1\right) + b^2 \quad (2)$$

where x_{Ni} indicates the normalized values in the range $(k_{min}, k_{max}) = (-1,1)$ and is calculated in Eq. (3) and Tansig function is shown in Eq. (4)

$$x_{Ni} = \frac{x_i - x_{min-i}}{x_{max-i} - x_{min-i}}(kmin_{max} + k_{min}) \quad (3)$$

$$\text{tansig}\left(\sum_{i=1}^{Ni} W^{12} x_{Ni} + b^1\right) = \frac{2}{1+e^{-2\left(\sum_{i=1}^{Ni} W^{12} x_{Ni} + b^1\right)}} - 1 \quad (4)$$

Note that N_n denoted in Eq. (1) is the normalized output. The predicted value is the reverse normalization of the normalized output and can be calculated by using Eq. (5).

$$N = (N_n - k_{\min})\frac{N_{0-\max} - N_{0-\min}}{k_{\max} - k_{\min}} + N_{0-\min} \quad (5)$$

Noted that, $x_{min\text{-}i}$, $x_{max\text{-}i}$, $N_{0\text{-}min}$, $N_{0\text{-}max}$ is the minimum and maximum value of input and output parameters of training data; N_i and N_h is the number of input and hidden neurons. Based on Eq. (2), the detail of the proposed empirical equation can be found in Appendix. The comparison between the borehole stability number (N) from FELA and the outcome from ANN prediction is represented in Fig. 13. It is obvious that if the points associated with the FELA and ANN prediction data are roughly the same, this point will be towards the middle of the line. The figure shows that the majority of the value points are close to the line, and the R^2 equal to 0.9997 further clarifies the optimal result of taking 6 neurons for training the ANN model.

It is interesting to adopt the weight of the optimal ANN model to do sensitivity analysis which is adopted in many previous studies[55-59] through Eq. (6)

$$I_j = \frac{\sum_{m=1}^{m=N_h}\left(\left(\frac{|W_{jm}^{ih}|}{\sum_{k=1}^{k=Ni}|W_{km}^{ih}|}\right)\times|W_{mn}^{ho}|\right)}{\sum_{k=1}^{k=N_i}\left\{\sum_{m=1}^{m=N_h}\left(|W_{km}^{ih}|/\sum_{k=1}^{k=N_i}|W_{km}^{ih}|\right)\times|W_{mn}^{ho}|\right\}} \quad (6)$$

where Ii denotes the relative importance of the i^h input variable on the output stability number (N), N_i and N_h are the number of input and hidden neurons, respectively; W is the connection weight; the superscripts i; h; and o refer to input, hidden, and output layers, respectively; the subscripts k; m; and n refer to input, hidden, and output neurons, respectively.

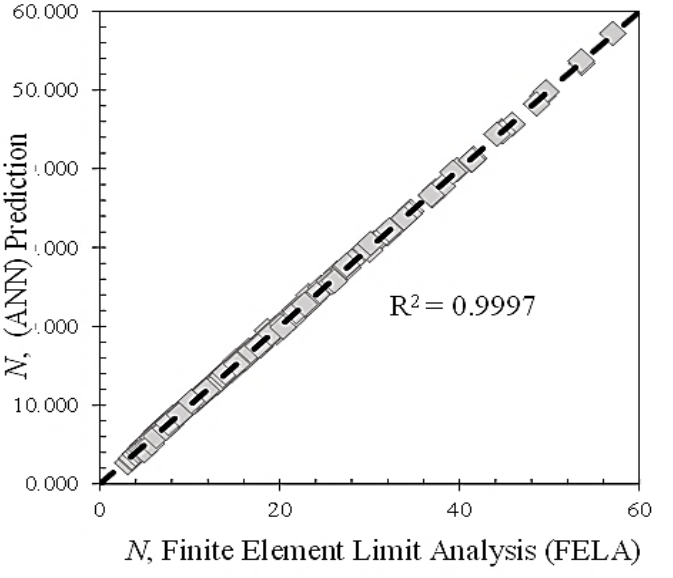

Fig. 13 Comparison between results from ANN prediction and FELA.

The relative importance of each input parameter, including depth ratio (H/D), anisotropic strength ratio (r_e), and dimensionless strength gradient ($\rho H/S_{uc0}$) on stability number (N) are shown in Fig. 14. It should be noted that the larger the

weight, the more important the corresponding input variable is to the output of the network. The results show that the depth ratio (H/D) is the most critical input variable in the ANN model, with a value of 56.20 %. The less essential parameters are dimensionless strength gradient ($\rho H/S_{uc0}$) and anisotropic strength ratio (r_e), with 25.50% and 18.29%, respectively. It is feasible to limit the number of input variables utilized in the model by selecting the H/D, which can simplify the model and reduce computational complexity.

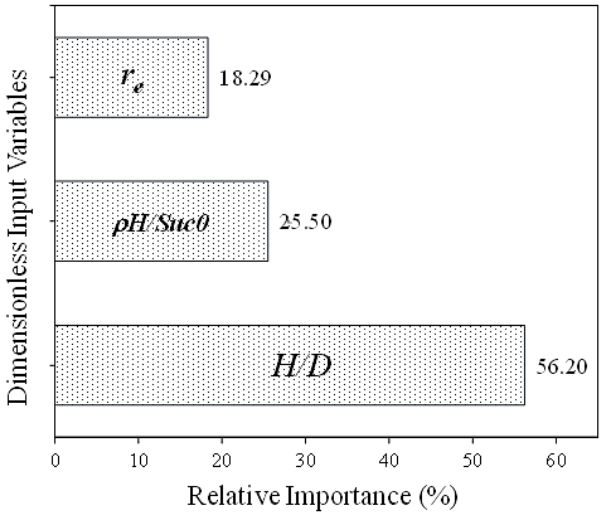

Fig. 14 Relative importance (%) of all input variables.

6. Conclusions

The present study has investigated the stability of boreholes with the slurry and its related failure mechanisms under slurry pressure in anisotropic and non-homogeneous clays. The axisymmetric upper and lower bound limit analysis were employed, with five iterations of adaptive meshing capacity, giving accurate bounding solutions, which were further averaged for results presentation. A series of the numerical study was then performed, and considerations are given to a linear increase in strength with borehole depth as well as the various governing parameters such as dimensionless strength gradient ($\rho H/S_{uc0}$), depth ratio (H/D), and anisotropic strength ratios (r_e). The study found that an increased H/D leads to nonlinearly increasing characteristics in the borehole stability number (N) and Factor of Safety (FS). Furthermore, an increase in $\rho H/s_{uc0}$ or r_e results in an increase in N and FS. The variables such as depth ratio (H/D), anisotropic strength ratio (r_e), and dimensionless strength gradient ($\rho H/S_{uc0}$) greatly affect the potential failure surfaces around the borehole. As a final step of the investigation, the proposed equation based on optimal gives well agreement with FELA results, where R^2=0.9997. The sensitivity analysis results showed that *H/D is the most important parameter while* $\rho H/S_{uc0}$ and r_e are later ranked at 56.20%, 25.50%, and 18.29%, respectively. The solutions presented in this study are applicable only to cylindrical boreholes in homogeneous soils and cannot be extended to rectangular or square boreholes or boreholes in layered soils. Future study may include a full 3D FELA analysis for investigating the borehole stability.

Acknowledgments

We acknowledge Ho Chi Minh City University of Technology (HCMUT), VNU-HCM for supporting this study. This research was funded by National Science, Research and Innovation Fund (NSRF), and King Mongkut's University of Technology North Bangkok with Contract no. KMUTNB-FF-66-12. This work was supported by the Thailand Science Research and Innovation Fundamental Fund fiscal year 2023.

Conflict of Interest

There is no conflict of interest.

Supporting Information

Not applicable.

Notations of parameters used in this study.

Notation	Meaning	Unit
H	Depth of borehole	m
D	Diameter of borehole	m
γ	Unit weight of clay	kN/m^3
γ_s	Unit weight of the slurry pressure	kN/m^3
ρ	Strength gradient	kPa/m
S_{uc0}	Undrained shear strength at the surface	kPa
r_e	Anisotropic strength ratio	Dimensionless
H/D	Depth ratio of the borehole	Dimensionless
$\rho H/S_{uc0}$	Strength gradient ratio	Dimensionless
FS	Factor of safety	Dimensionless
N	Borehole stability number	Dimensionless

References

[1] K. L. Nash, G. K. Jones, The support of trenches using fluid mud. In: Proc symp on grouts and drilling muds in engineering practice, Butterworths, London, 1963, 177-180.

[2] N. Morgenstern, I. Amir-Tahmasseb, The stability of a slurry trench in cohesionless soils, *Géotechnique*, 1965, **15**, 387-395, doi: 10.1680/geot.1965.15.4.387.

[3] G. M. Filz, T. Adams, R. R. Davidson, Stability of long trenches in sand supported by bentonite-water slurry, *Journal of Geotechnical and Geoenvironmental Engineering*, 2004, **130**, 915-921, doi: 10.1061/(asce)1090-0241(2004)130: 9(915).

[4] J.-S. Tsai, J.-C. Chang, Three-dimensional stability analysis for slurry-filled trench wall in cohesionless soil, *Canadian Geotechnical Journal*, 1996, **33**, 798-808, doi: 10.1139/t96-105-325.

[5] P. J. Fox, Analytical solutions for stability of slurry trench, *Journal of Geotechnical and Geoenvironmental Engineering*,

2004, **130**, 749-758, doi: 10.1061/(asce)1090-0241(2004)130: 7(749).
[6] Y.-C. Li, Q. Pan, P. J. Cleall, Y.-M. Chen, H. Ke, Stability analysis of slurry trenches in similar layered soils, *Journal of Geotechnical and Geoenvironmental Engineering*, 2013, **139**, 2104-2109, doi: 10.1061/(asce)gt.1943-5606.0000958.
[7] F. Zhang, Y. F. Gao, D. Leshchinsky, D. S. Zhu, G. H. Lei, Three-dimensional stability of slurry-supported trenches: end effects, *Computers and Geotechnics*, 2016, **74**, 174-187, doi: 10.1016/j.compgeo.2016.01.009.
[8] R. Saadi, M. Baheddi, N. Ferhoune, Analytical approach of the arching dual effect describing the stability of slurry-wall trenches in cohesionless soil, *International Journal of Geomechanics*, 2017, **17**, 04017081, doi: 10.1061/(asce)gm.1943-5622.0000973.
[9] P. Oblozinsky, K. Ugai, M. Katagiri, K. Saitoh, T. Ishii, T. Masuda, K. Kuwabara, A design method for slurry trench wall stability in sandy ground based on the elasto-plastic FEM, *Computers and Geotechnics*, 2001, **28**, 145-159, doi: 10.1016/s0266-352x(00)00028-8.
[10] E. Shalev, S. J. Bauer, M. A. Homel, T. H. Antoun, E. B. Herbold, O. Y. Vorobiev, H. Levin, G. Oren, V. Lyakhovsky, Borehole breakout modeling in arkose and granite rocks, *Geomechanics and Geophysics for Geo-Energy and Geo-Resources*, 2021, **7**, 1-23, doi: 10.1007/s40948-021-00215-y.
[11] C.-Y. Han, J.-H. Wang, X.-H. Xia, J.-J. Chen, Limit analysis for local and overall stability of a slurry trench in cohesive soil, *International Journal of Geomechanics*, 2015, **15**, doi: 10.1061/(asce)gm.1943-5622.0000268.
[12] J. Zhang, Y. Gao, F. Zhang, Y. Wan, M. Liu, Influence of anisotropy and nonhomogeneity on stability analysis of slurry-support trenches, *International Journal of Geomechanics*, 2018, **18**, 04018028, doi: 10.1061/(asce)gm.1943-5622.0001151.
[13] C. B. Qin, Determination of slurry density required for stability of slurry-supported trenches excavated in partially submerged soils, *Computers and Geotechnics*, 2019, **116**, 103212, doi: 10.1016/j.compgeo.2019.103212.
[14] H. Wang, M. Huang, Upper bound stability analysis of slurry-supported trenches in layered soils, *Computers and Geotechnics*, 2020, **122**, 103554, doi: 10.1016/j.compgeo.2020.103554.
[15] A. J. Li, R. S. Merifield, H. D. Lin, A. V. Lyamin, Trench stability under bentonite pressure in purely cohesive clay, *International Journal of Geomechanics*, 2014, **14**, 151-157, doi: 10.1061/(asce)gm.1943-5622.0000292.
[16] S. W. Sloan, Geotechnical stability analysis, *Géotechnique*, 2013, **63**, 531-571, doi: 10.1680/geot.12.rl.001.
[17] V. N. Khatri, J. Kumar, Stability of an unsupported vertical circular excavation in clays under undrained condition, *Computers and Geotechnics*, 2010, **37**, 419-424, doi: 10.1016/j.compgeo.2009.11.001.
[18] J. Kumar, D. Chakraborty, Stability numbers for an unsupported vertical circular excavation in c-ϕ soil, *Computers and Geotechnics*, 2012, **39**, 79-84, doi: 10.1016/j.compgeo.2011.08.002.
[19] J. Kumar, M. Chakraborty, J. P. Sahoo, Stability of unsupported vertical circular excavations, Journal of Geotechnical and Geoenvironmental Engineering, 2014, **140**, 358-366, doi: 10.1061/(asce)gt.1943-5606.0001118.
[20] B. Ukritchon, S. Keawsawasvong, A new design equation for drained stability of conical slopes in cohesive-frictional soils, *Journal of Rock Mechanics and Geotechnical Engineering*, 2018, **10**, 358-366, doi: 10.1016/j.jrmge.2017.10.004.
[21] W. Yodsomjai, S. Keawsawasvong, C. Thongchom, J. Lawongkerd, Undrained stability of unsupported conical slopes in two-layered clays, *Innovative Infrastructure Solutions*, 2020, **6**, 1-17, doi: 10.1007/s41062-020-00384-x.
[22] W. Yodsomjai, S. Keawsawasvong, S. Likitlersuang, Stability of unsupported conical slopes in hoek-brown rock masses, *Transportation Infrastructure Geotechnology*, 2021, **8**, 279-295, doi: 10.1007/s40515-020-00137-4.
[23] W. Yodsomjai, S. Keawsawasvong, T. Senjuntichai, Undrained stability of unsupported conical slopes in anisotropic clays based on anisotropic undrained shear failure criterion, *Transportation Infrastructure Geotechnology*, 2021, **8**, 557-568, doi: 10.1007/s40515-021-00153-y.
[24] V. Q. Lai, D. K. Nguyen, R. Banyong, S. Keawsawasvong, Limit analysis solutions for stability factor of unsupported conical slopes in clays with heterogeneity and anisotropy, *International Journal of Computational Materials Science and Engineering*, 2022, **11**, 2150030, doi: 10.1142/s2047684121500305.
[25] P. Petchkaew, S. Keawsawasvong, W. Tanapalungkorn, S. Likitlersuang, 3D stability analysis of unsupported rectangular excavation under pseudo-static seismic body force, *Geomechanics and Geoengineering*, 2023, **18**, 175-192, doi: 10.1080/17486025.2021.2019321.
[26] P. Petchkaew, S. Keawsawasvong, W. Tanapalungkorn, S. Likitlersuang, Seismic stability of unsupported vertical circular excavations in c-φ soil, *Transportation Infrastructure Geotechnology*, 2023, **10**, 165-179, doi: 10.1007/s40515-021-00221-3.
[27] V. Q. Lai, J. Shiau, S. Keawsawasvong, S. Seehavong, L. T. Cabangon, Undrained stability of unsupported rectangular excavations: anisotropy and non-homogeneity in 3D, *Buildings*, 2022, **12**, 1425, doi: 10.3390/buildings12091425.
[28] S. Keawsawasvong, J. Shiau, Instability of boreholes with slurry, *International Journal of Geosynthetics and Ground Engineering*, 2021, **7**, 1-11, doi: 10.1007/s40891-021-00326-2.
[29] C. C. Ladd, Stability evaluation during staged construction, *Journal of Geotechnical Engineering*, 1991, **117**, 540-615, doi: 10.1061/(asce)0733-9410(1991)117: 4(540).
[30] C. C. Ladd, D. J. DeGroot, Recommended practice for soft ground site characterization, Arthur Casagrande Lecture. In Proceedings of the 12th Panamerican Conference on Soil Mechanics and Geotechnical Engineering, Cambridge, 2003.
[31] S. Keawsawasvong, B. Ukritchon, Design equation for stability of a circular tunnel in anisotropic and heterogeneous clay, *Underground Space*, 2022, **7**, 76-93, doi: 10.1016/j.undsp.2021.05.003.

[32] K. Krabbenhøft, S. A. Galindo-Torres, X. Zhang, J. Krabbenhøft, AUS: Anisotropic undrained shear strength model for clays, *International Journal for Numerical and Analytical Methods in Geomechanics*, 2019, **43**, 2652-2666, doi: 10.1002/nag.2990.

[33] K. Krabbenhoft, A. V. Lyamin, Generalised Tresca criterion for undrained total stress analysis, *Géotechnique Letters*, 2015, **5**, 313-317, doi: 10.1680/jgele.15.00120.

[34] S. Keawsawasvong, J. Shiau, C. Ngamkhanong, V. Qui Lai, C. Thongchom, Undrained stability of ring foundations: axisymmetry, anisotropy, and nonhomogeneity, *International Journal of Geomechanics*, 2022, **22**, doi: 10.1061/(asce)gm.1943-5622.0002229.

[35] V. Q. Lai, J. Shiau, C. N. Van, H. D. Tran, S. Keawsawasvong, Bearing capacity of conical footing on anisotropic and heterogeneous clays using FEA and ANN, *Marine Georesources & Geotechnology*, 2022, 1-18, doi: 10.1080/1064119X.2022.2113485.

[36] S. Keawsawasvong, Bearing capacity of conical footings on clays considering combined effects of anisotropy and non-homogeneity, *Ships and Offshore Structures*, 2022, **17**, 2317-2328, doi: 10.1080/17445302.2021.1987110.

[37] S. Keawsawasvong, K. Yoonirundorn, T. Senjuntichai, Pullout capacity factor for cylindrical suction caissons in anisotropic clays based on anisotropic undrained shear failure criterion, *Transportation Infrastructure Geotechnology*, 2021, **8**, 629-644, doi: 10.1007/s40515-021-00154-x.

[38] D. K. Nguyen, T. P. Nguyen, S. Keawsawasvong, V. Q. Lai, Vertical uplift capacity of circular anchors in clay by considering anisotropy and non-homogeneity, *Transportation Infrastructure Geotechnology*, 2022, **9**, 653-672, doi: 10.1007/s40515-021-00191-6.

[39] V. Qui, Lai, Stability of limiting pressure behind soil gaps in contiguous pile walls in anisotropic clays, *Engineering Failure Analysis*, 2022, **134**, 106049, doi: 10.1016/j.engfailanal.2022.106049.

[40] E. van Oort, J. Nicholson, J. D'Agostino, Integrated Borehole Stability Studies: Key to Drilling at the Technical Limit and Trouble Cost ReductionAll Days. February 27-March 1, 2001. Amsterdam, Netherlands. SPE, 2001, **2**, 83-96, doi: 10.2118/67763-ms.

[41] O. K. Søreide, B. Bostrøm, P. Horsrud, Borehole stability simulations of an HPHT field using anisotropic shale modelling. 43rd U.S. Rock Mechanics Symposium and 4th U.S.-Canada Rock Mechanics Symposium, 2009.

[42] Y. Zhang, Study of borehole instability rule and the application in Sulige gas field. 2011 Asia-Pacific Power and Energy Engineering Conference. March 25-28, 2011, Wuhan, China. IEEE, 2011, 1-4, doi: 10.1109/APPEEC.2011.5748362.

[43] N. Ghasempour, M. Moosavi, M. Ali Aghighi, A micromechanical model to estimate borehole collapse pressure, *Periodica Polytechnica Civil Engineering*, 2017, **61**, 581, doi: 10.3311/ppci.9979.

[44] Jing-Sen, Cai, Design of borehole deployments for slope stability analysis based on a probabilistic approach, Computers and Geotechnics, 2021, **133**, 103909, doi: 10.1016/j.compgeo.2020.103909.

[45] Liqin, Ding, Borehole stability analysis: considering the upper limit of shear failure criteria to determine the safe borehole pressure window, *Journal of Petroleum Science and Engineering*, 2022, **212**, 110219, doi: 10.1016/j.petrol.2022.110219.

[46] R. Butterfield, Dimensional analysis for geotechnical engineers, Géotechnique, 1999, **49**, 357-366, doi: 10.1680/geot.1999.49.3.357.

[47] OptumCE 2019, OptumG2. Copenhagen, Denmark: Optum Computational Engineering. See https://optumce.com/ (accessed on 10 August 2019).

[48] Q. T. Huynh, V. Q. Lai, J. Shiau, S. Keawsawasvong, L. Z. Mase, H. T. Tra, On the use of both diaphragm and secant pile walls for a basement upgrade project in Vietnam, *Innovative Infrastructure Solutions*, 2021, **7**, 1-10, doi: 10.1007/s41062-021-00625-7.

[48] Q. T. Huynh, V. Q. Lai, J. Shiau, S. Keawsawasvong, L. Z. Mase, H. T. Tra, On the use of both diaphragm and secant pile walls for a basement upgrade project in Vietnam, *Innovative Infrastructure Solutions*, 2022, **7**, 17, doi: 10.1007/s41062-021-00625-7.

[49] L. Z. Mase, K. Amri, M. Farid, F. Rahmat, M. Nur Fikri, J. Saputra, S. Likitlersuang, Effect of water level fluctuation on riverbank stability at the estuary area of muaro kualo segment, muara bangkahulu river in bengkulu, Indonesia, *Engineering Journal*, 2022, **26**, 1-16, doi: 10.4186/ej.2022.26.3.1.

[50] L. Z. Mase, J. Saputra, A. F. Edriani, S. Keawsawasvong, V. Q. Lai, Finite element analysis to estimate bearing capacity of strip footing in coastal sandy soils in bengkulu city, Indonesia, *Engineering Journal*, 2022, **26**, 59-75, doi: 10.4186/ej.2022.26.5.59.

[51] L. Z. Mase, A. Perdana, Hardiansyah, K. Amri, S. Bahri, A case study of slope stability improvement in central bengkulu landslide in Indonesia, *Transportation Infrastructure Geotechnology*, 2022, **9**, 442-466, doi: 10.1007/s40515-021-00186-3.

[52] Q. T. Huynh, H. T. Tra, L. Z. Mase, N. H. Vo, V. Q. Lai, Analysing allowable horizontal displacements of retaining wall based on limited settlements of adjacent building, *Geotechnical Engineering*, 2022, **53**, 1-10.

[53] H. Ciria, J. Peraire, J. Bonet, Mesh adaptive computation of upper and lower bounds in limit znalysis, *International Journal for Numerical Methods in Engineering*, 2008, **75**, 899-944, doi: 10.1002/nme.2275.

[54] W. S. McCulloch, W. Pitts, A logical calculus of the ideas immanent in nervous activity, *The Bulletin of Mathematical Biophysics*, 1943, **5**, 115-133, doi: 10.1007/BF02478259.

[55] D. K. Nguyen, T. P. Nguyen, C. Ngamkhanong, S. Keawsawasvong, V. Q. Lai, Bearing capacity of ring footings in anisotropic clays: FELA and ANN, *Neural Computing and Applications*, 2023, **35**, 10975-10996, doi: 10.1007/s00521-023-08278-6.

[56] V. Q. Lai, W. Jitchaijaroen, S. Keawsawasvong, J. T. Chavda, W. Sae-Long, S. Limkatanyu, Application of ANN and FELA for

predicting bearing capacity of shell foundations on sand, *International Journal of Geosynthetics and Ground Engineering*, 2023, **9**, 1-13, doi: 10.1007/s40891-023-00437-y.
[57] J. Liu, Y. Jiang, W. Han, O. Sakaguchi, Optimized ANN model for predicting rock mass quality ahead of tunnel face using measure-while-drilling data, *Bulletin of Engineering Geology and the Environment*, 2021, **80**, 2283-2305, doi: 10.1007/s10064-020-02057-6.
[58] E. T. Mohamad, D. Jahed Armaghani, E. Momeni, S. V. Alavi Nezhad Khalil Abad, Prediction of the unconfined compressive strength of soft rocks: a PSO-based ANN approach, *Bulletin of Engineering Geology and the Environment*, 2015, **74**, 745-757, doi: 10.1007/s10064-014-0638-0.
[59] M. Koopialipoor, H. Tootoonchi, D. Jahed Armaghani, E. Tonnizam Mohamad, A. Hedayat, Application of deep neural networks in predicting the penetration rate of tunnel boring machines, *Bulletin of Engineering Geology and the Environment*, 2019, **78**, 6347-6360, doi: 10.1007/s10064-019-01538-7.
[60] M. T. Hagan, M. B. Menhaj, Training feedforward networks with the Marquardt algorithm, *IEEE Transactions on Neural Networks*, 1994, **5**, 989-993, doi: 10.1109/72.329697.
[61] J.-Y. Shim, J.-W. Zhang, H.-Y. Yoon, B.-Y. Kang, I.-S. Kim, Prediction model for bead reinforcement area in automatic gas metal arc welding, *Advances in Mechanical Engineering*, 2018, **10**, 168781401878149, doi: 10.1177/1687814018781492.

